Measuring supernova neutrino temperatures using lead perchlorate

S. R. Elliott
Department of Physics, Box 351560, University of Washington, Seattle, Washington 98195
(Received 5 June 2000; published 10 November 2000)

Neutrino interactions with lead produce neutrons in numbers that depend on neutrino energy and type. A detector based on lead perchlorate, for example, would be able to measure the energy deposited by electrons and gammas in coincidence with the number of neutrons produced. Sorting the electron energy spectra by the number of coincident neutrons permits the identification of the neutrino type that induced the reaction. This separation allows an analysis which can determine the temperatures of ν_e and $\bar{\nu}_e$ from a supernova in one experiment. The neutrino reaction signatures of lead perchlorate, and the fundamentals of using this material as a neutrino detector, are described.

PACS number(s): 97.60.Bw, 25.30.Pt

I. INTRODUCTION

Recently a number of groups have expressed an interest in using Pb as a target for neutrino interactions to study supernovae [1,2] or oscillations [3], and this inspired an estimate of the cross section [1]. The interest arises because of the large cross section and the low relative cost of Pb. As a result, additional cross section calculations were done recently by Fuller, Haxton, and McLaughlin [4] (hereafter referred to as FHM) and Kolbe and Langanke [5,6] (hereafter referred to as KL).

Interesting neutrino interactions with Pb consist of

$$\begin{aligned} \nu_e + {}^{208}\mathrm{Pb} \quad &\Rightarrow \quad {}^{208}\mathrm{Bi}^* + e^- \qquad \text{(CC)} \\ &\qquad \Downarrow \\ &\qquad {}^{208-y}\mathrm{Bi} + x\gamma + yn, \\ \nu_x + {}^{208}\mathrm{Pb} \quad &\Rightarrow \quad {}^{208}\mathrm{Pb}^* + \nu_x' \qquad \text{(NC)} \\ &\qquad \Downarrow \\ &\qquad {}^{208-y}\mathrm{Pb} + x\gamma + yn. \end{aligned}$$

Figure 1 shows the energetics of these transitions. The number of neutrons emitted (0, 1, or 2) depends on the neutrino energy, and on whether the transition is induced by charged current (CC) or neutral current (NC) interaction. The nuclear physics of this system was described in detail in Refs. [4,6].

An ideal lead-based neutrino detector would have an appreciable density of lead atoms and the capability of detecting the electrons, gammas, and neutrons produced in the reaction. Lead perchlorate [$Pb(ClO_4)_2$] has a very high solubility in water [500 g $Pb(ClO_4)_2$/ 100 g H_2O [7]], and the mixture is transparent. This transparency raises the hope that a Čerenkov detector can be assembled. Additionally, the presence of a neutron moderator (hydrogen) and a neutron capture nucleus (^{35}Cl) provides a method for observing the neutrons. The high-energy (8.6 MeV), neutron-capture γ rays from Cl would Compton scatter in the fluid and be observed via the Čerenkov light of the recoil electrons.

Supernovas emit on the order $10^{58}\nu$ of all types. The average energies of neutrinos emitted by a supernova follow a hierarchy, $\bar{E}_{\nu_e} < \bar{E}_{\bar{\nu}_e} < \bar{E}_{\nu_{\mu,\tau}}$ where $\nu_{\mu,\tau}$ indicates either μ or τ neutrinos and their antiparticles. The predicted values of the average energies for the three neutrino classes differ a great deal, and are estimated to be $\bar{E}_{\nu_e} = 11$ MeV, $\bar{E}_{\bar{\nu}_e} = 16$ MeV, and $\bar{E}_{\nu_{\mu,\tau}} = 25$ MeV [8,9].

Although not strictly thermal, the supernova neutrino energy spectra can be described well by a thermal distribution,

$$f_\nu = \frac{1}{T_\nu^3 F_2(\eta)} \frac{E_\nu^2}{\exp(E_\nu/T_\nu - \eta) + 1},$$

where f_ν is the normalized neutrino spectral shape, T_ν is an effective neutrino temperature, E_ν is the neutrino energy, and η is the degeneracy parameter (chemical potential divided by T_ν). For ν_e and $\bar{\nu}_e$, the supernova model predictions for the flux is well fit with $\eta = 3$, whereas for $\nu_{\mu,\tau}$ the flux is better described with $\eta = 0$. The normalization factor $F_2(\eta)$ has the values $F_2(0) = 1.803$ and $F_2(3) = 18.969$. The total neutrino fluence F_ν from a supernova can be estimated by

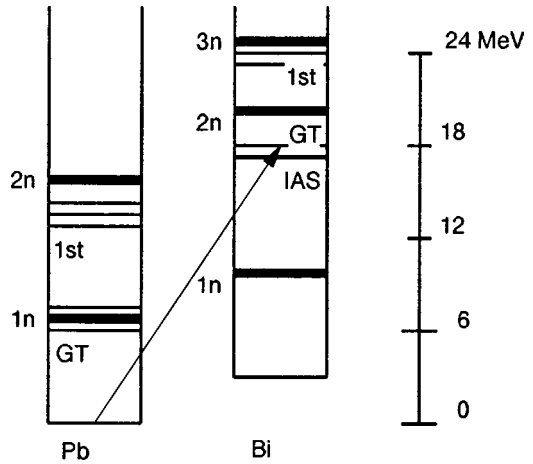

FIG. 1. The level scheme of a ^{208}Pb - ^{208}Bi system. The levels labeled GT indicate the Gamow-Teller resonance, IAS indicates the isobaric analog state, and *1st* indicates the states populated by first forbidden transitions. The one-, two-, and three-neutron emission thresholds are indicated by the labels *1n*, *2n*, and *3n*, respectively.

$$F_\nu = 2.8\times 10^{11}\ \mathrm{cm}^{-2}\,\frac{E_B}{10^{53}\ \mathrm{erg}}\,\frac{MeV}{T_\nu}\left(\frac{10kpc}{D}\right)^2,$$

where E_B, is the released energy, and D is the distance to the supernova.

The supernova ν_e spectrum is too soft to produce a large number of multiple-neutron inverse-β-decay events in Pb. However, if the higher energy $\nu_{\mu,\tau}$ oscillate into ν_e, the hardening of the spectrum will greatly alter the expected number of two-neutron events [4]. Thus the response of a Pb detector is intriguing because if T_{ν_e} is found to be larger than $T_{\bar{\nu}_e}$, it would be strong evidence that neutrino oscillations are taking place. However, the uncertainties in the neutrino energy distribution as predicted by the supernova models may complicate the interpretation of a measurement of the spectral parameters.

The FHM paper demonstrated that the NC and CC interaction rates in Pb are sensitive probes of T_{ν_μ,ν_τ}, T_{ν_e}, and $T_{\bar{\nu}_e}$. This paper further discusses the details of studying supernova neutrinos with Pb. In particular, the use of the added data arising from observing the product electrons and gammas in coincidence with neutrons is described. These data permit the separation of the NC and CC rates and a further division of CC ν_e and $\bar{\nu}_e$ events. This collection of data can be interpreted in terms of the three temperatures of interest. The CC event division is discussed here in detail. Although any Pb-based experiment that measures electrons, gammas, and neutrons might apply the techniques described herein, the example of using lead perchlorate as a target material is discussed.

II. PHYSICAL AND OPTICAL PROPERTIES

To build a reasonably large detector viewed by photomultiplier tubes from the periphery, the attenuation of the Čerenkov light must be minimal. Therefore the transmission of light through the medium is critical. To understand the transmission, measurements were made at several wavelengths through several concentrations of $Pb(ClO_4)_2$ [10]. The maximum achievable transmission is still under study, with attenuation lengths exceeding 2.5 m having been measured in an 80% solution. A large mass detector may require segmentation to minimize adverse effects from light loss.

The Čerenkov response of the medium depends on the index of refraction, which for $Pb(ClO_4)_2$ is 1.5 for an 80% solution by weight. The density of this solution is 2.7 g/cm^3, the corresponding ^{208}Pb number density is 1.7×10^{21}/cm^3, and the hydrogen number density is 3.6×10^{22}/cm^3. Some additional pertinent data for $Pb(ClO_4)_2$ are given in Table I.

The number of Čerenkov photons emitted by an energetic electron in $Pb(ClO_4)_2$ is about 185/cm [11] in the wavelength region of interest for phototubes. The stopping power of 80% (50%) $Pb(ClO_4)_2$ is about 0.2 cm/MeV (0.33 cm/MeV). Hence a 15-MeV electron will emit a total of about 550 (920) photons in 80% (50%) $Pb(ClO_4)_2$. Due to the modest light yield, the resolution ($\approx$20%) will be modest. The resonance widths will also contribute an uncertainty in relating the electron energy to the incoming neutrino energy by a comparable amount (a few MeV).

TABLE I. The neutron capture cross section for the various species in $Pb(ClO_4)_2$ the number of species in solution relative to Pb for an 80% solution concentration, and the neutron-capture rates relative to hydrogen.

Isotope	Neutron capture cross section (b)	Relative number density	Relative neutron capture rates
Pb		1.	
^{204}Pb	0.70	0.01	0
^{206}Pb	0.03	0.24	0
^{207}Pb	0.70	0.22	0.04
^{208}Pb	0.02	0.52	0
Cl		2.	
^{35}Cl	44.00	1.52	18.3
^{37}Cl	0.43	0.48	0.06
O		13.6	0
^{16}O	0.00	13.57	0
^{17}O	0.23	0.01	0
^{18}O	0.00	0.03	0
H	0.32	11.3	1
e^-	N.A.	234	N.A.

Because solutions of $Pb(ClO_4)_2$ contain a great deal of water and Cl, the neutron thermalization and capture time is of the order of 10–100 μs. This time scale is short compared to the ν detection rate during a supernova, but long enough to identify whether there are zero, one, or two neutrons in coincidence with a primary e^- or γ.

III. CROSS-SECTION MODELS

The FHM [4] paper pointed out the importance of the ^{208}Pb - ν cross section and the production of neutrons. They noted that the total number of neutrons produced by neutrino interactions with Pb is sensitive to the effective temperature of the supernova ν_e energy spectrum especially for reactions which produce multiple neutrons. However, they did not consider detection schemes that could measure the energy released in the form of electrons and gamma rays (hereafter referred to as the electromagnetic energy). Neutral current events release a large number of neutrons but very little electromagnetic energy. Hence NC events can be isolated from CC events by measuring the electromagnetic energy in coincidence with the neutrons.

The papers by FHM and KL provided effective cross sections for neutrino-lead interactions averaged over the neutrino energy spectra and summed over all the product nucleus states. It is just these distributions, however, which are needed to simulate the response of a detector and to optimize its design parameters. This section summarizes the nuclear physics model implemented to calculate these distributions. In Sec. IV, these distributions and their use in analyzing the neutrino spectra are described.

Specifically, the energy dependence of the five primary transitions of interest as identified by FHM is calculated: two

TABLE II. A description of the levels used in the simulation. The two-neutron rate from the NC first forbidden transition is not critical to the analysis. The neutron number branching ratios used here were motivated by results from FHM.

Transition	Product nucleus energy level with respect to Pb	Fraction decays with 0 n	Fraction decays with 1 n	Fraction decays with 2 n
CC IAS	17.53 MeV	0	1	0
CC GT	17.9 MeV	0	0.9	0.1
CC first forb.	24.1 MeV	0	0	1
NC GT	7.32 MeV	0.55	0.45	0
NC first forb.	14 MeV	0	~ 1	~ 0

for the NC interaction and three for the CC interaction. The parameters describing these transitions are given in Table II. For the isobaric analog state (IAS) CC and Gamow-Teller (GT) NC and CC transitions, the analytical expressions and matrix element values from Ref. [4] are used. For the first forbidden transitions, the cross section cannot be written in a closed form. Software to calculate that contribution to the cross section as used by FHM was obtained [18], and hence the cross-section calculations presented here agree with FHM by design.

Figure 2 shows the cross section overlaid on a normalized thermal flux distribution ($T_{\nu_e}=2.76$ MeV, $\eta=3$). Figure 3 shows the same for a higher neutrino temperature ($T_{\nu_e}=6.27$ MeV, $\eta=3$). The origin of the large increase in the interaction rate with temperature is clear from a comparison of these plots. The onset of the Pb cross section lies between these two temperature extremes. As a result, the interaction rate in Pb is highly sensitive to T_{ν_e}. This is especially true for the first forbidden transition, which leads to the emission of two neutrons.

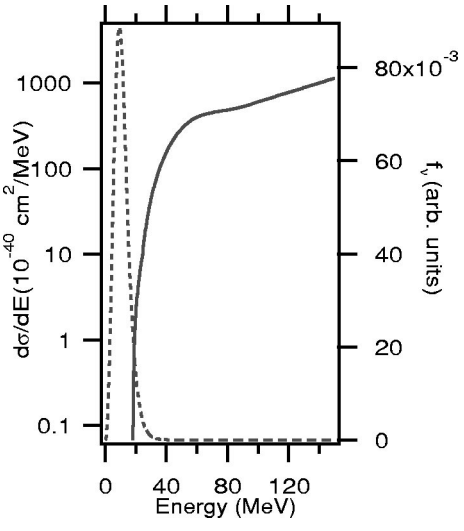

FIG. 2. The CC cross section as a function of energy is plotted on the left axis (solid line). A normalized thermal neutrino energy spectrum ($T_{\nu_e}=2.76$ MeV, $\eta=3$) is plotted on the right axis (dashed line). Note that the cross-section scale is logarithmic, whereas the spectrum scale is linear.

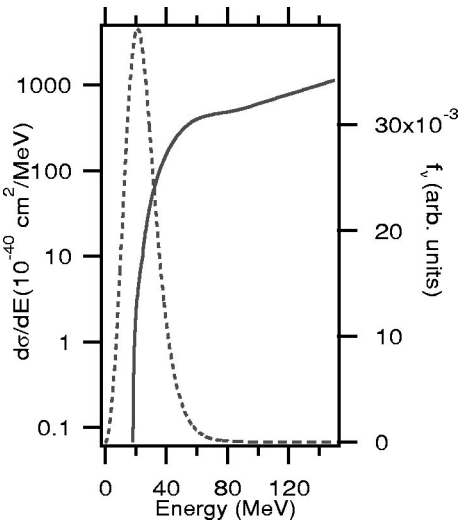

FIG. 3. The CC cross section as a function of energy plotted on the left axis (solid line). A normalized thermal neutrino energy spectrum ($T_{\nu_e}=6.27$ MeV, $\eta=3$) is plotted on the right axis (dashed line). Note that the cross-section scale is logarithmic, whereas the spectrum scale is linear.

Tables III and IV show some cross sections and relative interaction rates for the various components of $Pb(ClO_4)_2$. It is clear that the interactions with Pb and H dominate. Contributions from Cl, O, and elastic scattering of electrons are at the few percent level. The CC interaction of $\bar{\nu}_e$ on protons is a major contribution because the hydrogen density is large in $Pb(ClO_4)_2$ solutions. For other isotopes found in $Pb(ClO_4)_2$ but not listed in the table, FHM noted that the cross-section models vary like N-Z or NZ/A. For Pb, these

TABLE III. Cross sections for ν_e interactions on several isotopes, for various energy spectra and authors. The column labeled DAR indicates an average of the cross section over the muon decay-at-rest energy spectrum for electron neutrinos. The column labeled SN is for a Fermi-Dirac distribution of energies with $\eta=3$ and $T_\nu=6.266$ MeV ($\bar{E}_\nu \sim 25$ MeV). The cross sections are in units of 10^{-40} cm^2. For reference, various other cross sections are given.

Isotope	At 30 MeV	DAR	SN
$^{208}Pb(\nu_e,e^-)X$	31. [5], 44 [a]	59.6 [6]	34. [6], 47.5 [4]
$^{37}Cl(\nu_e,e^-)^{37}Ar$	1.0 [12]		
$^{35}Cl(\nu_e,e^-)X$			0.62 [4]
$^{35}Cl(\bar{\nu}_e,e^+)X$			0.14 [4]
$^{16}O(\nu_e,e^-)X$	0.01 [13]		0.11 [b] [13]
$^{16}O(\nu_x,\nu_x')X$			0.03 [5]
$D(\nu_e,e^-)X$	0.41 [14]	0.53 [15]	0.4 [14]
$H(\bar{\nu}_e,e^+)n$	0.6 [16]		0.5
$\nu_e(e,e')\nu_e'$	0.003 [17]		0.0023 [b] [13]

[a]This value was calculated by the author using the formalism of Ref. [4].

[b]This value is for $\eta=0$ and $T_\nu=8.0$ MeV.

TABLE IV. The neutrino interaction rates for 30-MeV ν_e for the dominant reactions. The values are given relative to ^{208}Pb. The cross-section value for Pb corresponds to that of FHM.

Element	Relative rate
$^{208}\mathrm{Pb}(\nu_e,e)$	100
$^{37}\mathrm{Cl}(\nu_e,e)$	2.0
$^{16}\mathrm{O}(\nu_e,e)$	0.6
$\mathrm{H}(\bar{\nu}_e,e^+)n$	32
$\nu_e(e,e')\nu_e'$	3.1

dependencies are small for the naturally occurring isotopes. Hence one can anticipate that their response to neutrinos will be similar. This is not the case for Cl. However, the difference in cross section between ^{35}Cl and ^{37}Cl is still probably smaller than other uncertainties and thus the Cl interaction rate is small.

IV. ELECTROMAGNETIC ENERGY

A detector based on lead perchlorate would be able to measure the energy deposited by e^- and γ in coincidence with the number of neutrons produced. The energy deposited in the detector due to e^- and γ is referred to here as the electromagnetic energy, to contrast it with that resulting from neutron capture. To identify a particular class of neutrinos, one sorts the electromagnetic energy spectra by the number of coincident neutrons. CC events always produce an electron which can have substantial energy in coincidence with neutrons. NC events produce either a high-energy γ with no neutrons or neutrons with little or no γ energy.

First consider the separation of NC from CC events. The product nucleus from the neutrino interaction can produce zero, one, or two neutrons. [Particle decays other than neutrons (alphas and protons) of the product nucleus states have a much lower branching ratio (see KL), and are ignored here.] When the interaction does produce a neutron, the neutrons carry away the available energy and there is little electromagnetic energy produced. Hence for the NC events, the electromagnetic energy is only appreciable when zero neutrons are emitted. Thus events which do have appreciable electromagnetic energy in coincidence with neutrons are indicative of ^{208}Pb - ν_e or H - $\bar{\nu}_e$ CC interactions.

Next consider the separation of the CC events into ν_e or $\bar{\nu}_e$ events. The two-neutron event rate is dominated by ν_e-induced CC transitions to the first forbidden level in Bi. Since the electromagnetic energy for the CC reactions is related to the incoming neutrino energy, the two-neutron event spectrum provides data on the incident ν_e energy spectrum. In contrast, the IAS and GT transitions induced by ν_e produce mostly one-neutron events. Furthermore, although $\bar{\nu}_e$ do not have an appreciable CC cross section on Pb, they have a large cross section on H. The one-neutron spectrum is therefore generated by reactions induced by ν_e and $\bar{\nu}_e$. But those are the only reactions that contribute significantly to the one-neutron electromagnetic energy spectrum, and therefore the one-neutron spectrum provides data on the $\bar{\nu}_e$ energy distribution. The two- and one-neutron spectra thus relate directly to the spectral features of the incident neutrino flux. Figures 4–7 show spectra of the electromagnetic energy for events in coincidence with one or two neutrons for two different neutrino energy distributions. These spectra have been convolved with an estimate for the detector resolution.

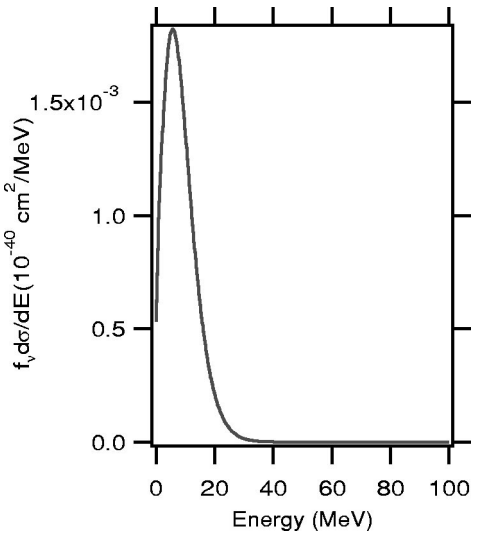

FIG. 4. The energy observed in the detector due to electrons from the CC interaction that are found in coincidence with two neutrons (E_2). This plot is for $T_{\nu_e}=2.76$ MeV and $\eta=3$.

For NC events, only GT excitations can produce an event with no neutrons as the resonance straddles the neutron separation energy. A γ ray of approximately 7.3 MeV is then emitted. This would produce a line in the zero-neutron electromagnetic energy spectrum. NC transitions can also produce one-neutron events and a modest number of two-neutron events. As there will be little electromagnetic energy in coincidence, the one-neutron events will be interpreted as

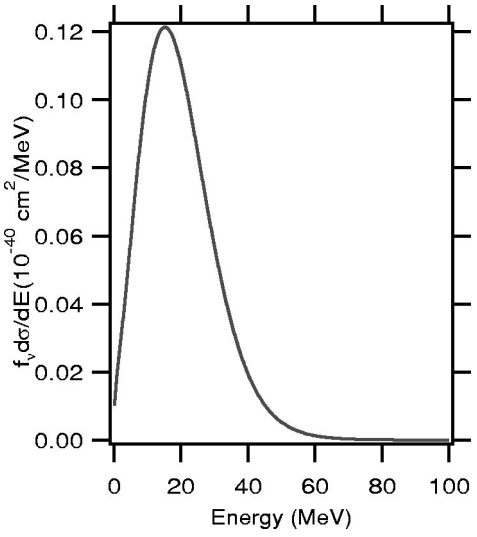

FIG. 5. The energy observed in the detector due to electrons from the CC interaction that are found in coincidence with two neutrons (E_2). This plot is for $T_{\nu_e}=6.27$ MeV and $\eta=3$.

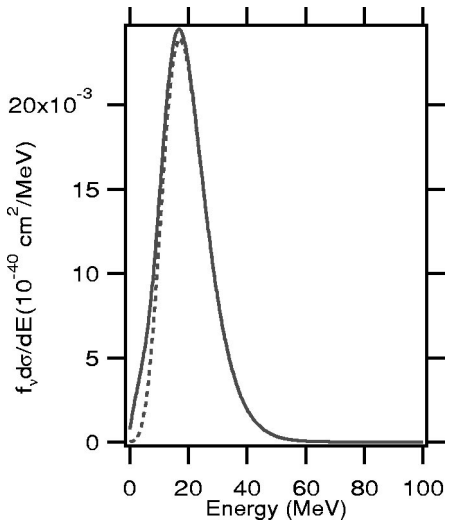

FIG. 6. The energy observed in the detector due to electrons from the CC interaction that are found in coincidence with one neutron (E_1). This plot is for $T_{\nu_e}=2.76$ MeV, $T_{\bar{\nu}_e}=4.01$ MeV, and $\eta=3$. The dashed line represents the contribution due to $\bar{\nu}_e$ on H.

an 8.6-MeV line in the zero-neutron spectrum. The strengths of these two lines in the zero-neutron spectrum provide a measure of the NC rate. Due to the resolution, these two lines will most likely be blended. These rates will be large even for low-temperature profiles.

One background to the CC one-neutron spectrum comes from two-neutron NC events. One of the two neutrons would be taken as a neutron, but the second would be mistaken for electromagnetic energy. For $T_{\nu_\mu,\nu_\tau}=6.27$, $T_{\nu_e}=2.76$, and

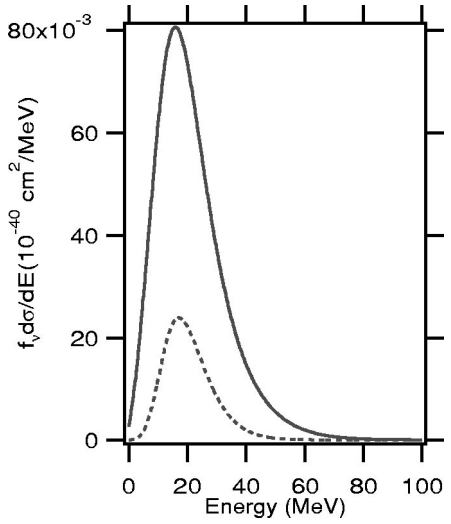

FIG. 7. The energy observed in the detector due to electrons from the CC interaction that are found in coincidence with one neutron (E_1). This plot is for $T_{\nu_e}=6.27$ MeV, $T_{\bar{\nu}_e}=4.01$ MeV, and $\eta=3$. The dashed line represents the contribution due to $\bar{\nu}_e$ on H.

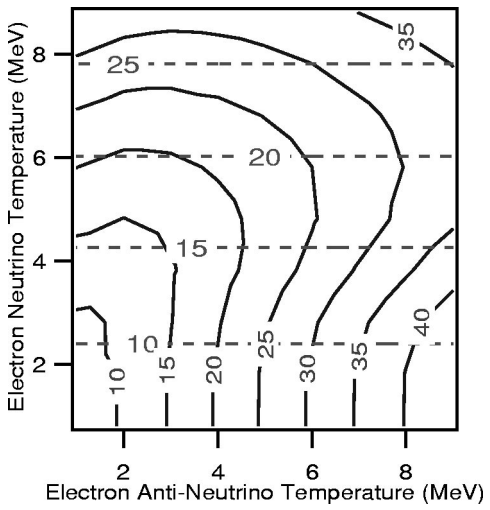

FIG. 8. A contour plot of $\bar{E}_1$ (solid lines) and $\bar{E}_2$ (dashed lines) as a function of the neutrino temperatures. In both cases, the average energy was calculated for events depositing at least 5 MeV.

$\eta=3$, the NC rate of two-neutron events will be comparable to the CC rate [4,6] because, although the NC cross section is much smaller, there are four times as many $\nu_{\mu,\tau}$'s as ν_e's and their temperature is much higher. Thus at low T_{ν_e}, this background must be separated. Note that because there are several γ sharing the energy and photons Compton scatter more than once before losing all their energy, the Cerenkov light produced by neutrons capturing on Cl will be isotropic in comparison to electrons from inverse beta decay. This could lead to a technique for separating this background. Otherwise an electromagnetic energy threshold of 10 MeV would eliminate it.

With the spectra in hand, one deduces the ν temperature by relating it to the average electromagnetic energy from the one-neutron spectrum ($\bar{E}_1$) and the two-neutron spectrum ($\bar{E}_2$) (Fig. 8). One also counts the total number of one-neutron events (N_1) and two-neutron events (N_2) in these spectra (Fig. 9). The ratio ($R=N_2/N_1$) depends strongly on the temperatures of the two types of neutrinos but is insensitive to uncertainties in the supernova distance scale. Using these parameters ($\bar{E}_1$, $\bar{E}_2$, N_2, N_1, R), the pair of neutrino temperatures that fit the data are determined.

If the electron neutrino temperature is clearly greater than that of the electron antineutrino temperature, it would be considered strong evidence for ν_e-ν_μ or ν_e-ν_τ oscillations. This condition is satisfied by the top left-hand section of these two-temperature plots. It should be noted that the contour plots were done for thermal spectra. If ν oscillates, the spectral shape could be complicated depending on the oscillation conditions, and this analysis would have to be extended.

To use this set of figures to determine the temperatures with some precision, one must estimate the uncertainty in the measured parameters. These uncertainties are mostly determined by the number of events observed. Regions in Figs. 8–10 are defined by the values of these parameters and their uncertainties. The boundaries of these regions indicated on

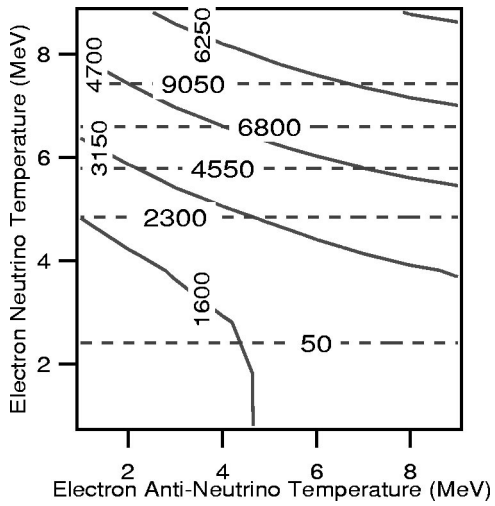

FIG. 9. This is a contour plot of the count rates as a function of the neutrino temperature for a 24-kt $Pb(ClO_4)_2$ detector. The solid lines are for the number of one-neutron CC events, and the dashed lines are for the number of two-neutron CC events. A threshold of 5 MeV was used.

the axes provide the corresponding temperature ranges that describe the data. For a commonly considered supernova at 10 kpc, with 3×10^{53} erg of released energy and a 10-kt Pb detector (24 kt of lead perchlorate), one expects to measure $\overline{E}_2=11.0\pm0.5$ MeV, $\overline{E}_1=19.6\pm0.2$ MeV, $N_1=1530$, $N_2=82$, and $R=0.053\pm0.006$ for nonoscillating spectra ($T_{\nu_e}=2.76$, $\eta=3$, $\overline{E}_{\nu_e}=11$, $T_{\bar{\nu}_e}=4.01$, $\eta=3$, and $\overline{E}_{\bar{\nu}_e}=16$). The uncertainties for the average energies were estimated by calculating the variance of the distribution, and dividing by the square root of the number of observed counts. The resulting statistical uncertainty in the temperatures is small, and the precision improves if T_{ν_e} is larger because the event rate is higher.

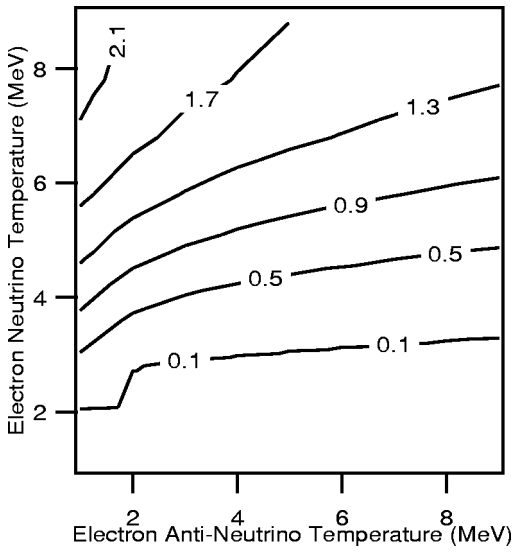

FIG. 10. This a contour plot of R as a function of the neutrino temperatures. R is the ratio of two-neutron events to one-neutron events. A threshold of 5 MeV was used.

TABLE V. Some cross-section comparisons between FHM and KL. The cross sections are given in units of 10^{-40} cm^2. In most cases the two calculations have fair agreement. The selection here was chosen to emphasize the differences.

Transition and spectral input	FHM	KL
$Pb(\nu_e,e)X$ $T_{\nu_e}=4.0$ MeV, $\eta=3$.	6.9	6.7
$Pb(\nu_e,e)X$ $T_{\nu_e}=8.0$ MeV, $\eta=0$.	58	43
$Pb(\nu,\nu')X$ $T_{\nu_e}=4.0$ MeV, $\eta=3$.	0.66	0.23
$Pb(\nu,\nu')X$ $T_{\nu_e}=8.0$ MeV, $\eta=0$.	4.5	1.4
$Pb(\nu,e)X$ π^+ decay at rest	91 [a]	59.6

[a]This value was calculated by the author using the formalism of FHM.

V. SUMMARY

The Sudbury Neutrino Observatory (SNO) [19] and Super-Kamiokande (SK) [20] experiments are operating. In the event of a supernova, Super-Kamiokande experiments will observe a large number of $\bar{\nu}_e$-H events ($\sim$10000 for $T_{\bar{\nu}_e}=4.01$, $\eta=3$) and SNO will observe a number of ν_e-D events ($\sim$90 for $T_{\nu_e}=2.76$, $\eta=3$). The average energy measured for these two reactions could be compared in a two-temperature plot in a similar analysis as described above. Due to the smaller number of events, the uncertainty comparing these energy distributions would be determined by the SNO measurement. For these ν temperatures, a 24-kt $Pb(ClO_4)_2$ experiment would count a number of two-neutron ν_e events comparable to the number of SNO $D(\nu_e,e^-)pp$ events. Thus the average energy analysis of a $Pb(ClO_4)_2$ experiment would have a sensitivity similar to the SNO-SK comparison. But the total number of counts in a $Pb(ClO_4)_2$ experiment is much more sensitive to the neutrino temperatures. SNO [$Pb(ClO_4)_2$] observed about three (60) times as many $D(\nu_e,e^-)pp$ (two-neutron) events at $T_{\nu_e}=6$ than at 2.76 MeV. This extra handle on the data adds a powerful redundancy to the analysis.

It is obvious from Table V that there are still large uncertainties in the nuclear physics of these interactions. Furthermore, reactions on the other Pb isotopes were not considered, although they would tend to increase the signal. Therefore, the response of such a detector should be measured in a prototype. The ν_e spectrum from a stopped μ^+ decay is comparable to that from supernovae. Thus the two- and one-neutron spectra could be measured at a beam stop facility [21] without the influence of $\bar{\nu}_e$. Since the $\bar{\nu}_e$-proton reaction is well understood, it does not need additional study and the measurement would focus on what is currently poorly known: the nuclear physics parameters of the lead reactions. Thus the theoretical uncertainties in the cross section could be diminished by a beam stop experiment.

The details of the analysis presented in this paper will alter as the nuclear physics of this system becomes better

known. But the general conclusions generic to lead detectors will not. It is very powerful to measure not just the total number of neutrons produced but the two- and one-neutron rates separately. Furthermore the observation of electrons and γ rays in coincidence with the neutrons can permit the separation of NC and CC interactions. If one observes a supernova with a Pb detector, these combinations of data can be analyzed to estimate the temperatures of the neutrino spectra.

ACKNOWLEDGMENTS

I would like to thank Peter Doe, Hamish Robertson, Thomas Steiger, John Beacom, Edwin Kolbe, Gail McLaughlin, and George Fuller for useful conversations. I am especially grateful to Wick Haxton for providing code to estimate the first forbidden transition cross section. This research was support by the U.S. Department of Energy, Grant No. DE-FG03-97ER41020.

[1] C. K. Hargrove *et al.*, Astropart. Phys. **5**, 183 (1996).
[2] D. B. Cline *et al.*, Phys. Rev. D **50**, 720 (1994); P. F. Smith, Astropart. Phys. **8**, 27 (1997).
[3] C. K. Hargrove (private communication).
[4] George M. Fuller, Wick C. Haxton, and Gail C. McLaughlin, Phys. Rev. D **59**, 085005 (1999).
[5] E. Kolbe (private communication).
[6] E. Kolbe and K. Langanke, nucl-th/0003060.
[7] *Handbook of Chemistry and Physics*, 65th ed., edited by R. C. West (CRC Press, Boca Raton, FL, 1984).
[8] D. S. Miller, J. R. Wilson, and R. W. Mayle, Astrophys. J. **415**, 278 (1993).
[9] H.-T. Janka and W. Hillebrant, Astron. Astrophys. **224**, 49 (1989).
[10] P. J. Doe, S. R. Elliott, C. Paul, and R. G. H. Robertson, Nucl. Phys. B (Proc. Suppl.) **87**, 512 (2000).
[11] C. Caso *et al.*, Eur. Phys. J: Appl. Phys. **3**, 1 (1998).
[12] T. Kuramoto, M. Fukugita, Y. Kohyama, and K. Kubodera, Nucl. Phys. **A512**, 711 (1990).
[13] W. C. Haxton, Nucl. Instrum. Methods Phys. Res. A **264**, 37 (1988).
[14] K. Kubodera and S. Nozawa, Int. J. Mod. Phys. E **3**, 101 (1994).
[15] S. Ying, W. C. Haxton, and E. M. Henley, Phys. Rev. C **45**, 1982 (1992).
[16] P. Vogel, Phys. Rev. D **29**, 1918 (1984); P. Vogel and J. F. Beacom, *ibid.* **60**, 053003 (1999).
[17] John N. Bahcall, *Neutrino Astrophysics* (Cambridge University Press, Cambridge, 1989).
[18] W. C. Haxton (private communication).
[19] J. Boger *et al.*, Nucl. Instrum. Methods Phys. Res. A **449**, 172 (2000).
[20] Y. Fukuda *et al.*, Phys. Rev. Lett. **82**, 2430 (1999).
[21] F. T. Avignone *et al.*, the ORLaND Collaboration, in *Perspectives in Nuclear Physics*, edited by J. H. Hamilton, H. K. Carter, and R. B. Piercy (World Scientific, Singapore, 1999), pp. 25–34.